An aqueous solution-based doping strategy for large-scale synthesis of Sb-doped ZnO nanowires

2011 Nanotechnology 22 225602

(http://iopscience.iop.org/0957-4484/22/22/225602)

Nanotechnology **22** (2011) 225602 (8pp) doi:10.1088/0957-4484/22/22/225602

An aqueous solution-based doping strategy for large-scale synthesis of Sb-doped ZnO nanowires

Fei Wang[1,2], Jung-Hun Seo[3], Dylan Bayerl[1], Jian Shi[1], Hongyi Mi[3], Zhenqiang Ma[3], Deyin Zhao[4], Yichen Shuai[4], Weidong Zhou[4] and Xudong Wang[1,5]

[1] Department of Materials Science and Engineering, University of Wisconsin at Madison, USA
[2] Department of Chemistry, University of Wisconsin at Madison, Madison, USA
[3] Department of Electrical and Computer Engineering, University of Wisconsin at Madison, USA
[4] Department of Electrical Engineering, University of Texas at Arlington, USA

E-mail: xudong@engr.wisc.edu

Received 23 December 2010, in final form 14 March 2011
Published 1 April 2011
Online at stacks.iop.org/Nano/22/225602

Abstract

An aqueous solution-based doping strategy was developed for controlled doping impurity atoms into a ZnO nanowire (NW) lattice. Through this approach, antimony-doped ZnO NWs were successfully synthesized in an aqueous solution containing zinc nitrate and hexamethylenetetramine with antimony acetate as the dopant source. By introducing glycolate ions into the solution, a soluble antimony precursor (antimony glycolate) was formed and a good NW morphology with a controlled antimony doping concentration was successfully achieved. A doping concentration study suggested an antimony glycolate absorption doping mechanism. By fabricating and characterizing NW-based field effect transistors (FETs), stable p-type conductivity was observed. A field effect mobility of 1.2 $cm^2\ V^{-1}\ s^{-1}$ and a carrier concentration of $6 \times 10^{17}\ cm^{-3}$ were achieved. Electrostatic force microscopy (EFM) characterization on doped and undoped ZnO NWs further illustrated the shift of the metal–semiconductor barrier due to Sb doping. This work provided an effective large-scale synthesis strategy for doping ZnO NWs in aqueous solution.

(Some figures in this article are in colour only in the electronic version)

1. Introduction

Doping semiconductor nanowires (NWs) with foreign elements to manipulate their electrical and magnetic properties is an important aspect for the realization of various types of advanced nanodevices [1]. Although most semiconductor NWs are synthesized and doped from the vapor phase, *in situ* doping in the solution synthesis of semiconductors offers several unique advantages, such as low cost, mass production and ease of processing [2]. In the colloidal synthesis of semiconductor quantum dots, doping can be achieved by adding a particular amount of a suitable dopant precursor together with the host material's precursors [3, 4]. For NW materials that are synthesized from aqueous solution, *in situ* doping to manipulate their properties while maintain their one-dimensional (1D) growth behavior has been challenging.

ZnO NWs, as an important wide-bandgap semiconductor nanostructure building block, has attracted extensive research interest [5–7]. The growth of ZnO NWs from either the vapor phase or aqueous solution can be repeatedly executed [5, 8, 9]. One main obstacle to high-performance ZnO NW-based electronic/optoelectronic devices is the challenge to realize stable and low-resistance p-type ZnO NWs. A few reports have been released on successful syntheses of p-type ZnO NWs using nitrogen or phosphorus doping via vapor methods [10, 11]. Furthermore, arsenic (As) and antimony (Sb) have been suggested as promising dopant candidates that

[5] Author to whom any correspondence should be addressed.

might produce more stable p-type conductivity and higher hole concentrations. It was suggested that an As(or Sb)$_{Zn}$–2V$_{Zn}$ complex would be an acceptor with low formation energy and ionization energy [12, 13]. Inspired by the prediction, a considerable effort has been made on doping ZnO using As or Sb via CVD and molecular beam epitaxy (MBE) [14–16]. The solution-based growth of Sb-doped ZnO nanorods was also reported recently, but with poor morphology control and an unknown transport property [17].

In this paper, we report a simple and well-controlled aqueous solution-based doping strategy for the synthesis of single-crystalline Sb-doped ZnO NWs. Glycolate was identified as an effective coordinating ligand that controlled the releasing of Sb ions during the formation of ZnO NWs so that both reasonable doping and good NW morphology were successfully achieved. The doping concentration control was also studied under different experimental parameters, from which an Sb glycolate absorption mechanism was proposed to explain the Sb doping process. A stable p-type transport property was revealed by characterizing single NW-based field effect transistors (FETs) and further confirmed by electrostatic force microscopy (EFM) measurements.

2. Experimental section

2.1. Synthesis and structural characterizations of undoped and Sb-doped ZnO NWs

Undoped and Sb-doped zinc oxide NWs were grown on silicon substrates. The substrate was first coated with a layer of zinc oxide as seed. To do this, a few drops of 5 mM zinc acetate ethanol solution were dropped on the silicon substrates and blown dry. After repeating this step three times, the substrate was baked in air for 20 min at 350 °C. It was then placed on the surface of the nutrient solution and the reaction was conducted at 90 °C for a day. The nutrient solution for growing the undoped ZnO NWs (solution 1) consisted of 25 mM sodium nitrate and 25 mM hexamethylenetetramine (HMT). The nutrient solution for growing the Sb-doped ZnO NWs (solution 2) was prepared by adding a certain amount of dopant solution into solution 1 before the growth. The dopant solution was prepared by mixing equal molar sodium hydroxide and glycolic acid ($C_2H_4O_3$) to form sodium glycolate ($NaC_2H_3O_3$), followed by dissolving antimony acetate ($SbAc_3$) in the sodium glycolate. In all the experiments, we kept the ratio of antimony acetate to glycolate at 1:12. In a typical synthesis the amount of Sb was 0.2% in molar ratio with respect to that of zinc.

The Sb doping concentration was studied with inductively coupled plasma (ICP) atomic emission spectroscopy (AES). The test samples were prepared by dissolving the Sb-doped ZnO NWs in 0.10 M glycolic acid. A control solution was prepared by dissolving a ZnO seed layer of exactly the same substrate size in 0.10 M glycolic acid to assess the contribution from the seed layer. Therefore, the calibrated zinc and Sb concentrations are both contributed by the NWs only. A standard sample was made by dissolving 1.00×10^{-3} M zinc nitrate and 1.00×10^{-5} M antimony acetate in 0.10 M glycolic acid solution to determine the relationship between emission intensity and sample concentration.

2.2. Characterization

The morphology and structural characterizations of the ZnO NWs were performed by scanning electron microscopy (SEM; LEO 1530), transmission electron microscopy (TEM; Philips CM200UT) and a Hi-Star 2D x-ray diffractometer. A low-temperature photoluminescence (PL) study of undoped and Sb-doped nanowires was carried out using an UV LED with a central wavelength of 365 nm.

NW-based FETs with a back-gate configuration were used to characterize the electrical transport property of ZnO NWs. 100 nm thick SiO_2 was deposited by plasma enhanced chemical vapor deposition (PECVD) on a heavily doped silicon substrate and acted as the gate dielectric. NWs were transferred onto the SiO_2/Si substrate, followed by a treatment in oxygen plasma to remove possible organics on the NWs. To activate the p-type dopants, an Sb-doped NW sample was annealed at 850 °C in atmosphere for 30 min before the transfer. Ti (30 nm)/Au(120 nm) source and drain electrodes were defined by photolithography and deposited with electron-beam (e-beam) evaporation, followed by a liftoff. The distance between the source and the drain electrodes was typically 1–2 μm. To prevent the NWs from absorbing oxygen molecules or other contaminants from the environment, 100 nm SiO_2 and 50 nm Si_3N_4 layers were deposited as a passivation layer for the sample by e-beam evaporation and PECVD, respectively [18]. The current–voltage characteristics of the single NW-FETs were measured using a semiconductor parameter analyzer (HP4155B) in the dark to avoid any light induced photocurrents. EFM characterizations were performed with a Park Systems XE-70 atomic force microscope. Phosphorus-doped silicon cantilever probes with a 20 nm thick Cr sublayer and 20 nm thick Au conductive coating were used for EFM imaging.

3. Results and discussions

3.1. Synthesis design and Sb-doped NW morphology

In a typical aqueous solution system for ZnO NW growth, hexamethylenetetramine (HMT) acts as a buffer and hydrolyzes slowly in water, generating ammonia. Thus the pH value of the nutrient solution is gradually increased, which induces the precipitation of ZnO. To grow doped ZnO NWs from an aqueous solution, one key issue is to incorporate dopant ions onto the growing ZnO surface with a controlled rate. This requires not only a soluble dopant source, so that the doping concentration can be controlled, but also a slow dopant release rate to prevent the dopant from precipitating all at once. However, there are hardly any Sb salts that are both water soluble and compatible with the ZnO growth solution, mainly because Sb is extremely easy to hydrolyze in water.

It is known that trivalent Sb can form coordinate compounds with α-hydroxycarboxylate ligands, where each ligand forms a five-membered chelating ring [19]. Therefore, ligands that fall in this family would be able to dissolve

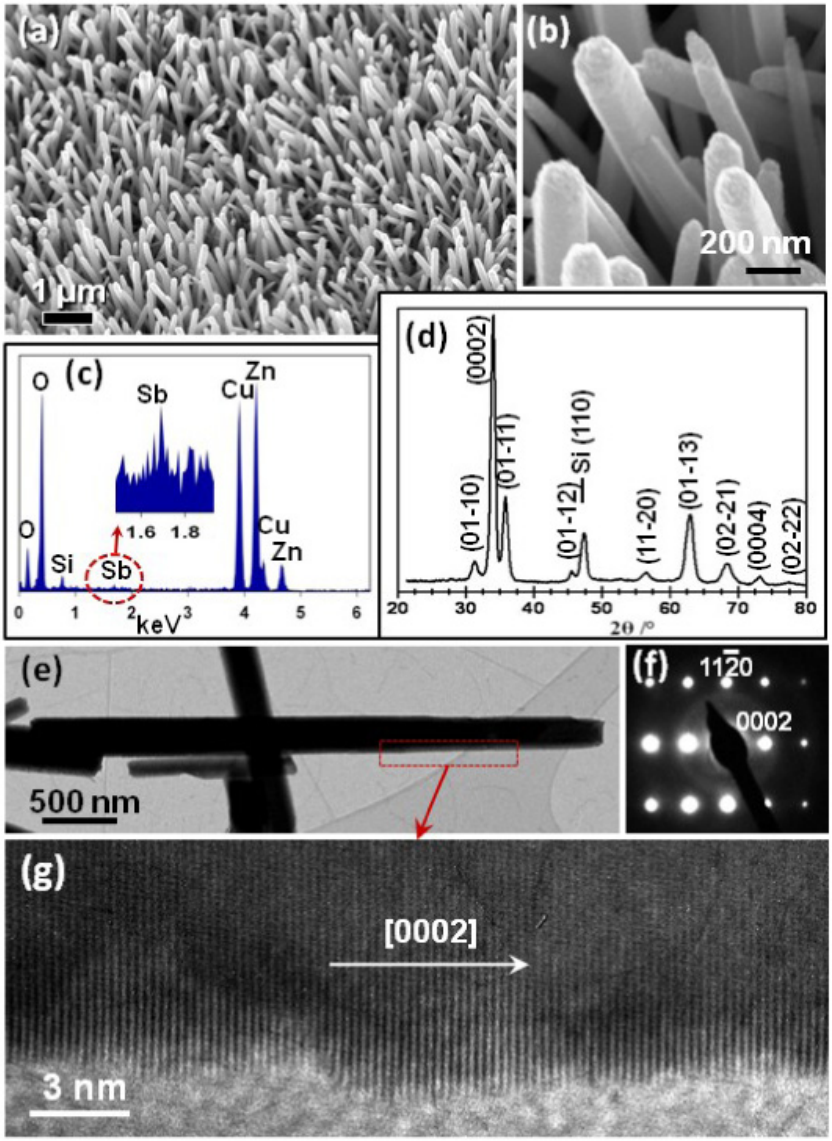

Figure 1. Morphological and structural characterization of Sb-doped ZnO nanowires using antimony acetate and sodium glycolate. (a) SEM image of the as-grown Sb-doped NWs. (b) A magnified SEM image; (c) EDS of Sb-doped ZnO NWs taken under TEM; (d) x-ray diffraction spectrum of as-synthesized Sb-doped ZnO NW arrays; (e) TEM image of Sb-doped ZnO NWs; (f) the corresponding SAED pattern. (g) HR-TEM showing the dislocation-free lattice of an Sb-doped ZnO NW.

insoluble Sb salts and prevent Sb^{3+} from hydrolyzing in the initial neutral environment of the reaction solution. This strategy would help resolve the issue of Sb solubility and thus lead to controlled incorporation of Sb. In our research, two types of such ligands, citrate and glycolate, were studied. $SbAc_3$ dissolved in both sodium citrate and sodium glycolate solutions and formed clear dopant solutions, which were added to the original nutrient solution for Sb doping. EDS revealed that Sb was successfully incorporated into the ZnO crystals, whereas distinguishing morphologies were achieved in the presence of two different ligands. Sodium citrate produced ZnO platelets that were stacked together. The formation of this morphology was believed to result from the preferential absorption of citrate ions on ZnO crystal surfaces, which significantly altered the growth rate along different crystal orientations [20].

On the other hand, glycolate, as the simplest member in the family of α-hydroxycarboxylate ligands, successfully preserved the NW morphology, while stabilizing the Sb^{3+} in ZnO nutrient solution. Figure 1(a) shows the as-grown Sb-doped ZnO NWs distributed on a silicon substrate. The NWs are on average $\sim$4 μm long and $\sim$100–200 nm in diameter with a hexagonal cross-section, as shown in figure 1(b). The existence of Sb in the doped NWs was confirmed by the energy-dispersive x-ray spectrum (EDS), as shown in figure 1(c). No sodium signal was observed from the EDS. It is a common phenomenon that impurities can dramatically affect the growth behavior of crystals, although there is not yet a generally accepted theory to explain the mechanisms by which impurities participate in the crystallization process [21, 22]. Our results suggest that sodium and glycolate ions have negligible effect on the growth behavior of ZnO crystals in

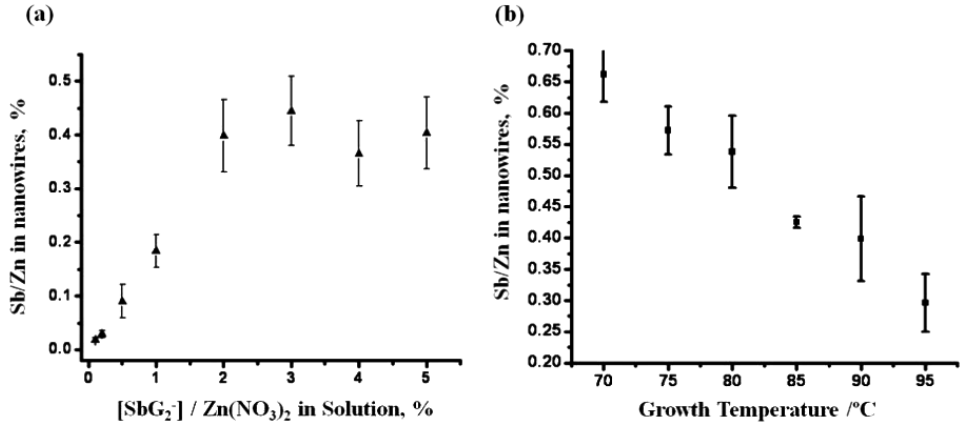

Figure 2. Doping concentration versus different experimental parameters. (a) Doping concentration dependence on added concentration of SbG_2^- while the temperature was kept at 90 °C; (b) doping concentration dependence on growth temperature while the added concentration of antimony glycolate was kept at 0.5 mM, which was 2% of the concentration of zinc nitrate.

aqueous solutions. This statement was further proved by control experiments in which undoped ZnO NWs were grown unaffected by the presence of sodium glycolate without $SbAc_3$. However, a slower growth rate of Sb-doped NWs was observed compared to the undoped ones. This is possibly due to the incorporation of Sb ions onto the growing surfaces of ZnO, which rendered the growth steps less reactive or inoperative.

The wurtzite crystal structure of Sb-doped ZnO NWs was first confirmed by x-ray diffraction as shown in figure 1(d). The intense (0002) peak indicated the quasi-aligned NW orientation. The peak positions of undoped ZnO nanowires looked identical to doped ones at the resolution of our instrument. The TEM image shown in figure 1(e) revealed that the surfaces of the as-synthesized NWs were rather clean. The corresponding selective-area electron diffraction (SAED) pattern evidenced the single-crystalline structure of the Sb-doped NWs, which grew along the [0001] direction (figure 1(f)). No destruction of the ZnO crystal lattice due to the incorporation of Sb was observed from the Sb-doped ZnO NWs, as shown by the high-resolution TEM image in figure 1(g), although the side surface was not perfectly flat.

3.2. Control of Sb doping concentration

In order to study the formation mechanism of Sb-doped ZnO nanowires, the Sb doping concentration was studied with different growth parameters. We first kept the growth temperature at 90 °C and the concentration of zinc nitrate and HMT at 25 mM, while using antimony glycolate (SbG_2^-) with a concentration varying from 0.1% to 5% of the concentration of added zinc nitrate. A linear increase of the doping concentration in ZnO NWs was observed with the increase of antimony glycolate concentration ($[SbG_2^-]$) when it was below 2%. Higher $[SbG_2^-]$ (>2%) exhibited a saturated effect on the doping concentration (figure 2(a)). Experiments were also conducted by varying the temperatures from 70 °C to 95 °C and keeping $[SbG_2^-]$ at 2%. The doping concentration in ZnO NWs decreased almost linearly when the temperature was increased (figure 2(b)).

In the solution synthesis of colloidal quantum dots and nanoparticles, it is believed that *in situ* doping is through dopant species being absorbed onto the growing surface of the host materials and then becoming buried by the growing host materials [3, 23]. According to our experimental results, we propose that Sb doping is achieved by SbG_2^- coordinating ions being absorbed on the growing ZnO surfaces, followed by glycolate ligands (HG^-) being desorbed and antimony ions being buried by upcoming host material (ZnO). Based on this proposed mechanism, higher concentrations of SbG_2^- coordinating ions would lead to more absorption of SbG_2^- ions. Thus higher doping concentrations would be received. This explains why the doping concentration increased linearly with the concentrations of added dopant solution (figure 2(a)), in which SbG_2^- was the dominant Sb species. Due to the existence of the equilibrium between SbG_2^- in the nutrient solution and SbG_2^- absorbed on the ZnO surface, the absorbed SbG_2^- would increase linearly with the SbG_2^- added to the nutrient solution before saturation. Finally, when the concentration of SbG_2^- is greater than 2% of zinc nitrate (i.e. 0.5 mM), the absorption of SbG_2^- reached saturation, indicating a possible saturated absorption of SbG_2^- coordinating ions on the growing ZnO surfaces.

While we acknowledge that Sb^{3+} ions could also possibly be absorbed and thus contribute to doping, we ruled out the possibility that free Sb^{3+} ions were the major absorbed species because the concentration of free Sb^{3+} ions decreased with the concentration of added dopant solution. Consider the coordination equilibrium between Sb^{3+} and SbG_2^- ions:

$$Sb^{3+} + 2HG^- + 2OH^- \leftrightarrow SbG_2^- + 2H_2O, \qquad (1)$$

where HG^- denotes glycolate ion ($HOCH_2COO^-$) and the ligand $G(^-OCH_2COO^-)$ in the coordinating compound has one less hydrogen atom (figure 3).

$$K_{eq} = \frac{[SbG_2^-]}{[Sb^{3+}][HG^-]^2[OH^-]^2}. \qquad (2)$$

In our doping solution, we always kept the ratio of antimony acetate to sodium glycolate at 1:12. Therefore, since

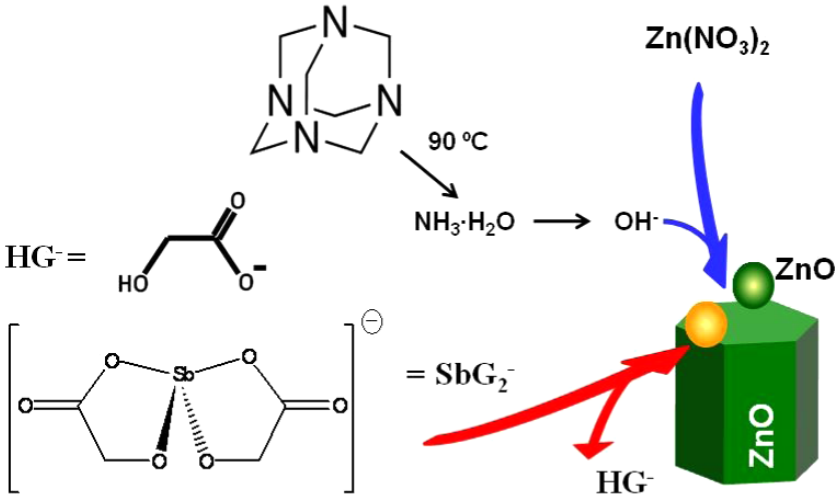

Figure 3. Molecular structure of SbG_2^- and a schematic diagram showing the incorporation of Sb into ZnO. SbG_2^- ions diffuse to the growing ZnO NWs surface and get absorbed. HG^-'s leave the surface thereafter.

SbG_2^- is the dominant Sb species after we dissolved antimony acetate in sodium glycolate, the ratio of SbG_2^- to HG^- is always 1:10. Thus,

$$[Sb^{3+}] = \frac{1}{10K_{eq}[HG^-][OH^-]^2}, \quad (3)$$

In addition, the pH value of the nutrient solution was found to be almost constant (varied within 6.00 and 6.10) at different dopant concentrations. Therefore, under a constant temperature, more dopants would bring more HG^- and less concentration of Sb^{3+} would exist. Similarly, the concentration of antimony hydroxyl species ($Sb(OH)_x^{+(3-x)}$) would also decrease when more dopant solution was added. Therefore, if Sb^{3+} ions or $Sb(OH)_x^{+(3-x)}$ were the major antimony species that were absorbed on the growing ZnO surface, the doping concentration would have decreased with the increased amount of dopant concentration; this contradicts the experimental observation. Similar processes that involve Sb^{3+} or $Sb(OH)_x^{+(3-x)}$, such as the hydrolysis of Sb, could not be the main mechanism that was responsible for our doping process.

Using the SbG_2^- absorption mechanism, the dependence of the doping concentration on temperature can also be explained. Since the absorption of SbG_2^- on the ZnO growing surface is an exothermic process, a lower temperature is favorable for absorption. Therefore, a higher doping concentration of Sb was observed as the reaction temperature was decreased from 95 to 70 °C (figure 2(b)). Figure 3 shows the molecular structure of SbG_2^- and the schematic process of doping Sb into ZnO NWs. Our results indicated that the addition of glycolate ligands not only resolved the Sb solubility issue but also helped the incorporation of Sb into the ZnO crystal. By adjusting the amount of dopant solution and the growth temperature, the Sb doping concentration is easily controlled.

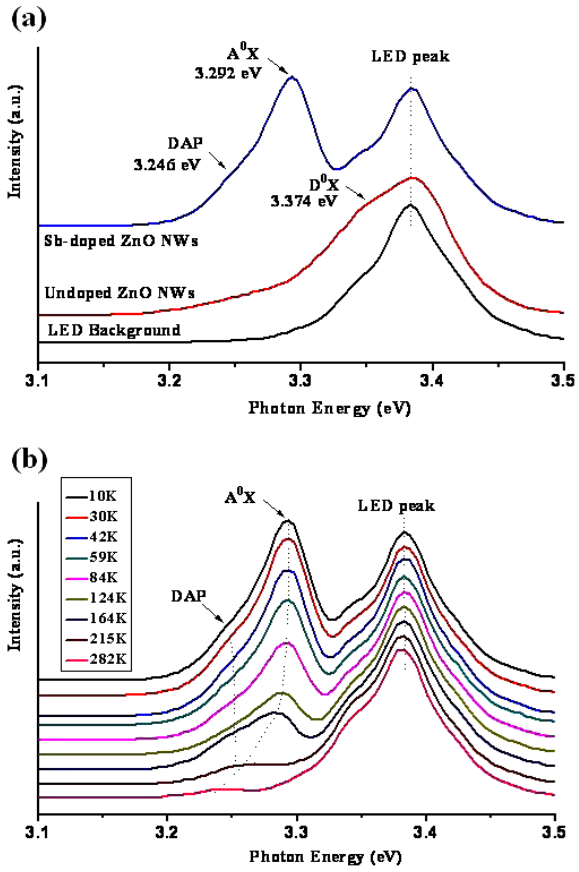

Figure 4. Low-temperature photoluminescence of Sb-doped NWs. (a) Doped NWs, undoped NWs and LED background at 10 K; (b) temperature dependence.

3.3. Optical and electrical properties

To study the optical properties of Sb-doped ZnO NWs, a low-temperature PL study was carried out. Figure 4(a) shows the PL spectra of Sb-doped, undoped NWs as well as the light source background at 10 K. In the spectrum of Sb-doped nanowires, the peak at 3.292 eV was assigned to the neutral-acceptor-bound exciton (A^0X) transition and the

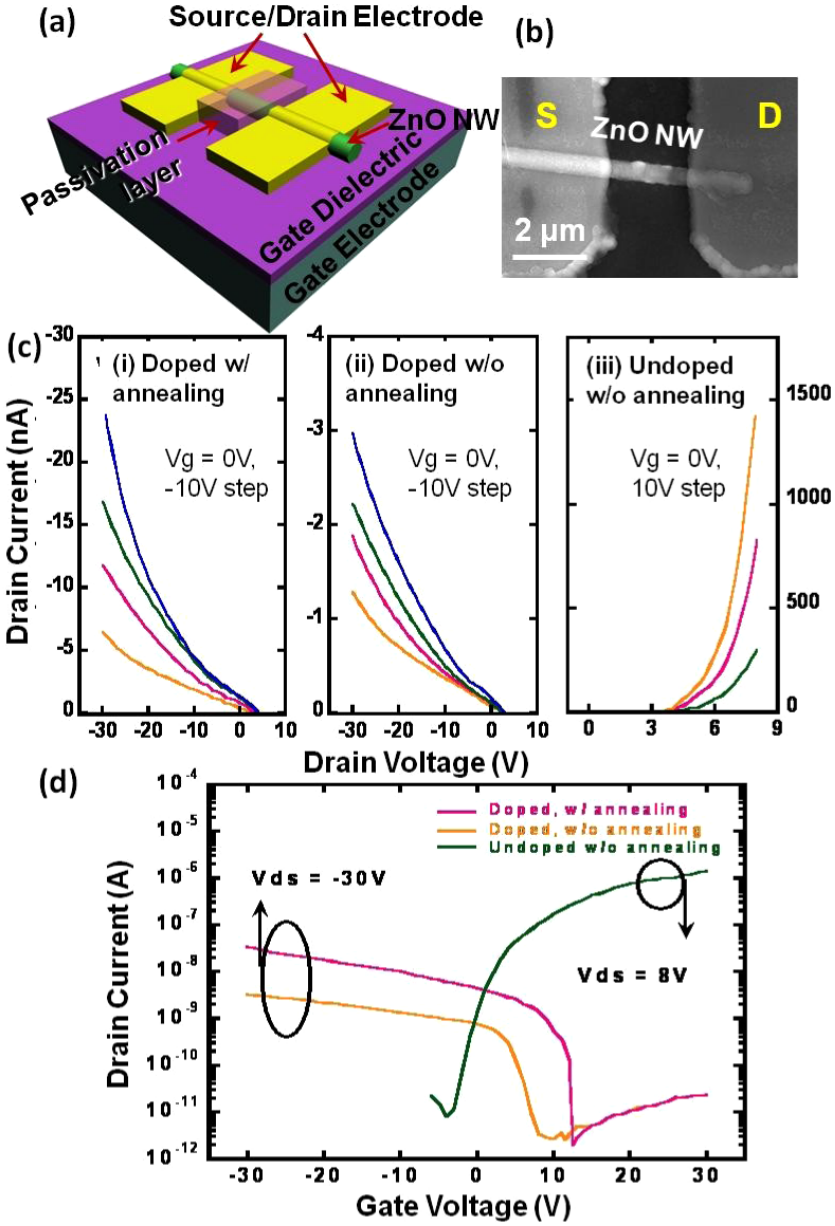

Figure 5. (a) Schematic diagram of a ZnO NW-based FET. (b) An SEM image of a ZnO NW-based FET. (c) The drain current (I_{ds}) versus the drain voltage (V_{ds}) graphs obtained from NW-FETs made from Sb-doped ZnO annealed at 850 °C (left); Sb-doped ZnO without annealing (center); and undoped ZnO (right). (d) Log versus the gate voltage (V_g) graph obtained with $V_{ds} = -30$ for Sb-doped ZnO and $V_{ds} = 8$ V for undoped ZnO.

peak at 3.246 eV was assigned to the donor–acceptor pair (DAP) transition. In the spectrum of undoped nanowires as a comparison, a near-band edge emission associated with the neutral-donor-bound exciton (D^0X) was observed at about 3.374 eV. We also investigated the photon energy of A^0X and DAP emissions at different temperatures (figure 4(b)). We noted that the A^0X and DAP emissions merged together at higher temperatures due to thermal ionization. These peaks and their temperature variations were also observed in the reports on Sb-doped ZnO prepared by high-temperature vacuum techniques [24, 25].

The electric transport property of Sb-doped ZnO NWs was studied by characterizing single NW-based FETs with a back-gate configuration, as shown in figure 5(a). The detailed structure of this device has been described in section 2. The corresponding SEM image of such a device after coating the passivation layer is shown in figure 5(b). The diameter of the NWs was ∼200–250 nm and the channel length was ∼2 μm.

To compare the doping results, both Sb-doped (annealed and as-grown) and undoped ZnO NWs (as-grown) were measured. Figure 5(c) shows current versus drain–source bias (I_{ds}–V_{ds}) curves of the NW-FETs obtained under different gate voltages (V_g starting at 0 V and increase at 10 V steps) varying from 10 to −30 V for Sb-doped ZnO NW-FETs and from 0 to 10 V for undoped ZnO NW. The field effect mobility (μ_0) and carrier concentration (n_e) of the ZnO NW-FETs were derived using the cylinder-on-an-infinite-plate model via the following equations: $\mu = L^2 g_m / C_i V_{ds}$ and $n_h = V_{th} C_i / q\pi L (d/2)^2$,

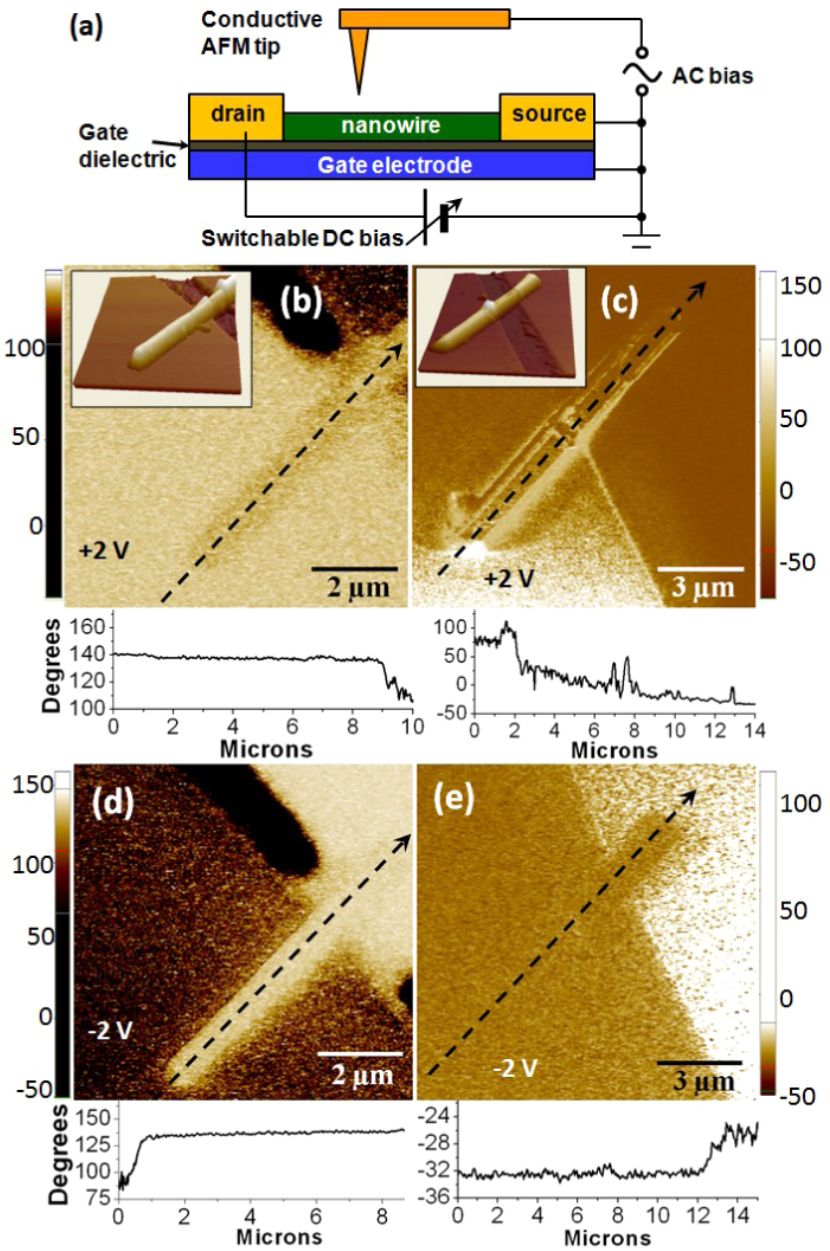

Figure 6. (a) Schematic drawing of the experimental setup for EFM characterization. EFM phase images of an undoped ZnO NW ((b) and (d)) and a Sb-doped NW ((c) and (e)). Corresponding topography images are shown in the insets of (b) and (c), respectively. The drain biases are indicated in the bottom left of each image. The line profiles under each image show the magnitude of the phase shift along the corresponding black dashed arrows, which pass through the NWs.

where $C_i = 2\pi\varepsilon_0\varepsilon_{SiO_2}L/\ln(4h/d)$ is the NW capacitance; L and d is the effective length and diameter of the NW; g_m, V_{ds}, and V_{th}, is the transconductance, the source–drain voltage, and the threshold voltage, respectively [26]. As shown in figures 5(c) and (d), the undoped ZnO NW-FET showed typical n-type characteristics with a threshold voltage of −2.2 V, a mobility of 1.2 $cm^2\ V^{-1}\ s^{-1}$ and a carrier concentration of $1.3 \times 10^{17}\ cm^{-3}$. The transfer characteristic showed an on/off ratio of 10^5. The as-grown Sb-doped ZnO NW-FETs exhibited strong p-type characteristics. An on/off ratio of 10^3, a threshold voltage of −8.1 V, a mobility of 0.03 $cm^2\ V^{-1}\ s^{-1}$, and a carrier concentration of $4.8 \times 10^{17}\ cm^{-3}$ were observed from an un-annealed sample. By annealing the doped sample at 850 °C for 30 min, the on/off ratio, carrier concentration and mobility increased to 10^4, $6.0\times10^{17}\ cm^{-3}$ and 1.2 $cm^2\ V^{-1}\ s^{-1}$, respectively (figures 5(c) and (d)).

EFM was performed on the single NW-based FETs to further verify the conduction type of the ZnO NWs. The characterization setup is schematically shown in figure 6(a). Topography and EFM phase images were recorded simultaneously during scans of Sb-doped and undoped NW-based FETs with $V_{ds} = \pm2$ V and $V_g = 0$ V. The EFM phase shift is proportional to the arcsine of the square of the local potential difference between the surface and the cantilever tip [27]. The contrast in EFM phase images therefore corresponds to

the local variation in surface potential and indicates where significant voltage drops occur in the scans of NW-based FETs under nonzero V_{ds} [28]. Figures 6(b) and (d) are EFM phase images of an undoped NW-FET, while figures 6(c) and (e) are of the Sb-doped NW-FET. The corresponding topography images of both EFTs are shown in the insets of figures 6(b) and (c), respectively. The drain bias was applied on the left-hand side electrode (drain) and the right-hand side electrode (source) was grounded. The largest EFM phase shifts were observed between the NW ends and the corresponding electrodes, which are the source electrode in figures 6(b) and (e), and the drain electrode in figures 6(c) and (d). This large phase shift indicates which NW-electrode junction has the largest voltage drop due to formation of a potential barrier.

The switching of the potential distribution allowed us to identify the conduction type of the semiconductor NWs. For the n-type (undoped ZnO) NW-FET, a +2 V drain bias rendered an forward bias at the drain electrode contact, thus little potential change was detected along the entire NW but a sharp potential drop was identified at the source electrode contact, as shown in figure 6(b). When a −2 V drain voltage was applied, the contact between the drain electrode and the NW became reversely biased, thus the abrupt voltage drop was detected at the drain electrode side, as shown in figure 6(d). When switching to a Sb-doped ZnO NW, the bias condition between the NW and source/drain electrodes was reversed. A large voltage drop occurred at the drain electrode contact when a +2 V drain bias was applied (figure 6(c)); while a −2 V drain bias produced a potential barrier at the source electrode contact (figure 6(d)). The inversion of the potential barrier under the same drain bias clearly shows the difference in the conduction types between the doped and the undoped ZnO NWs. The transport measurements and EFM results showed that the solution-based Sb doping method is able to produce p-type ZnO NWs with a reasonably good transport property, which are feasible to integrate with undoped ZnO (n-type) made from the same procedure to form homogeneous ZnO p–n junctions.

4. Conclusion

In summary, Sb-doped ZnO NWs were successfully synthesized in an aqueous solution using antimony acetate as the dopant source. Sodium glycolate was added as a coordinating ligand to dissolve antimony acetate and form antimony glycolate coordinating ions. An antimony glycolate absorption mechanism was proposed based on the Sb doping concentration dependence on various experimental parameters. The new doping mechanism enables a control of the doping concentration by varying the concentration of antimony glycolate and/or the growth temperature. By fabricating and characterizing single NW-based FETs, stable p-type conductivity was observed. A carrier mobility of 1.2 $cm^2\ V^{-1}\ s^{-1}$ and a carrier concentration of $6 \times 10^{17}\ cm^{-3}$ were achieved. The p-type conductivity of the Sb-doped ZnO NWs was further confirmed by EFM. This study provides a large-scale synthesis method for effectively doping ZnO nanostructures, and thus tailoring their optical and electronic properties.

Acknowledgments

The authors thank Professor John F Berry for helpful discussions. This research is supported by NSF CMMI-0926245, AFOSR PECASE award under grant number FA9550-091-0482 (program manager: Dr Gernot Pomrenke), and ARO W911NF-09-1-0505 (program manager: Mike Gerhold).

References

[1] Lauhon L J, Gudiksen M S and Lieber C M 2004 *Phil. Trans. R. Soc.* **362** 1247–60
[2] Yuhas B D, Zitoun D O, Pauzauskie P J, He R R and Yang P D 2006 *Angew. Chem. Int. Edn* **45** 420–3
[3] Erwin S C, Zu L J, Haftel M I, Efros A L, Kennedy T A and Norris D J 2005 *Nature* **436** 91–4
[4] Beaulac R, Archer P I, Ochsenbein S T and Gamelin D R 2008 *Adv. Funct. Mater.* **18** 3873–91
[5] Wang Z L 2004 *J. Phys.: Condens. Matter* **16** R829–58
[6] Huang M H, Mao S, Feick H, Yan H Q, Wu Y Y, Kind H, Weber E, Russo R and Yang P D 2001 *Science* **292** 1897–9
[7] Ohta H, Kawamura K, Orita M, Hirano M, Sarukura N and Hosono H 2000 *Appl. Phys. Lett* **77** 475
[8] Vayssieres L 2003 *Adv. Mater.* **15** 464–6
[9] Greene L E, Law M, Goldberger J, Kim F, Johnson J C, Zhang Y F, Saykally R J and Yang P D 2003 *Angew. Chem. Int. Edn* **42** 3031–4
[10] Xiang B, Wang P W, Zhang X Z, Dayeh S A, Aplin D P R, Soci C, Yu D P and Wang D L 2007 *Nano Lett.* **7** 323–8
[11] Lu M P, Song J, Lu M Y, Chen M T, Gao Y, Chen L J and Wang Z L 2009 *Nano Lett.* **9** 1223–7
[12] Limpijumnong S, Zhang S B, Wei S H and Park C H 2004 *Phys. Rev. Lett.* **92** 155504
[13] Wahl U, Correia J G, Mendonca T and Decoster S 2009 *Appl. Phys. Lett.* **94** 215503
[14] Guan H S, Xia X C, Zhang Y T, Gao F B, Li W C, Wu G G, Li X P and Du G T 2008 *J. Phys.: Condens. Matter* **20** 292202
[15] Xiu F X, Yang Z, Mandalapu L J, Zhao D T, Liu J L and Beyermann W P 2005 *Appl. Phys. Lett.* **87** 152101
[16] Guo W, Allenic A, Chen Y B, Pan X Q, Che Y, Hu Z D and Liu B 2007 *Appl. Phys. Lett.* **90** 242108
[17] Briscoe J, Gallardo D E and Dunn S 2009 *Chem. Commun.* 1273–5
[18] Chang P C, Chien C J, Stichtenoth D, Ronning C and Lu J G 2007 *Appl. Phys. Lett.* **90** 133101
[19] Reza M Y, Hossain M M, Karim M R, Tarafder M T H and Hughes D L 2010 *Acta Crystallogr.* E **66** M116–U328
[20] Tian Z R R, Voigt J A, Liu J, McKenzie B, McDermott M J, Rodriguez M A, Konishi H and Xu H F 2003 *Nat. Mater.* **2** 821–6
[21] Davey R J 1976 *J. Crys. Growth* **34** 109–19
[22] Davis K J, Dove P M and De Yoreo J J 2000 *Science* **290** 1134–7
[23] Pradhan N, Goorskey D, Thessing J and Peng X G 2005 *J. Am. Chem. Soc.* **127** 17586–7
[24] Przezdziecka E, Kaminska E, Pasternak I, Piotrowska A and Kossut J 2007 *Phys. Rev.* B **76** 193303
[25] Xiu F X, Yang Z, Mandalapu L J, Zhao D T and Liu J L 2005 *Appl. Phys. Lett.* **87** 252102
[26] Goldberger J, Sirbuly D J, Law M and Yang P 2005 *J. Phys. Chem.* B **109** 9–14
[27] Lei C H, Das A, Elliott M and Macdonald J E 2004 *Nanotechnology* **15** 627–34
[28] Gudiksen M S, Lauhon L J, Wang J, Smith D C and Lieber C M 2002 *Nature* **415** 617–20